Biointerface Research in Applied Chemistry
Open-Access Journal (ISSN: 2069-5837)

Article
Volume 14, Issue 4, 2024, 93
https://doi.org/10.33263/BRIAC144.093

Screening and Formation Thermodynamics of Co-Crystal: Salicyclic Acid-Benzamide Co-Crystal System Case Study

Pooja Bhimshankar Sarsambi [1], Vaishali Choudhary [2], Abhinav Joseph [2,*], Pawan Gupta [3,*]

[1] School of Education, Lovely Professional University, Phagwara-144411, Punjab, India; poojasarsambi6@gmail.com;
[2] School of Chemical Engineering and Physical Sciences, Lovely Professional University, Phagwara-144411, Punjab, India; vaishalichaudhary708@gmail.com (V.C.); abhinav.24349@lpu.co.in (A.J.);
[3] Department of Pharmaceutical Chemistry, Shri Vile Parle Kelavani Mandal's Institute of Pharmacy, Dhule-424001, Maharashtra, India; pawanpharma79@hotmail.com;
* Correspondence: abhinav.24349@lpu.co.in (A.J.); pawanpharma79@hotmail.com (P.G.);
Scopus Author ID 42161510800
Received: 10.07.2023; Accepted: 20.12.2023; Published: 21.07.2024

Abstract: Selecting a suitable co-former is the most important aspect of co-crystal design. Several knowledge-based, computational, and experimental techniques are available to guide the search for novel co-crystals. However, most are based on complex methodologies, are not readily accessible, and demand high computational costs. Moreover, when used solely, they do not guarantee that co-crystals with the predicted structures will form. In this work, a step-by-step approach towards co-crystal screening involving well-established knowledge-based methods and commonly available analytical techniques is illustrated using salicylic acid-benzamide co-crystal as a model system. The approach quickly and reliably predicted the formation of stoichiometrically diverse co-crystals between salicylic acid and benzamide. The thermodynamic formation functions necessary to understand the nature of co-crystallization were estimated for salicylic acid-benzamide (1:1) co-crystal using a predictive model based on the melting point and sublimation thermodynamic data. The formation of the co-crystal was found to be endothermic and entropy-driven.

Keywords: co-crystal; co-former; screening; synthon; ΔpKa rule; mechanochemistry; formation thermodynamics.

1. Introduction

Organic compounds can exist in crystalline and amorphous forms (Figure 1). For commercial applications, crystalline forms are preferred over amorphous forms due to their better stability, handling, and storage characteristics during various manufacturing stages. In the pharmaceutical industry, almost 80% of the active pharmaceutical ingredients (APIs) are manufactured in crystalline form except in some circumstances where using an amorphous form is desirable, such as for improving solubility. In recent years, the interest in crystalline forms has expanded to incorporate single-component as well as multi-component crystals. Single-component crystals include anhydrous or non-solvated form of an API and their polymorphic modifications. Multi-component crystals comprise an API with different intermolecular interactions with another molecule or ion, forming new crystal forms without affecting the covalent chemistry. This group includes hydrates, solvates, salts, co-crystals, and combinations. Additionally, polymorphs may also exist for each multi-component crystal [1].

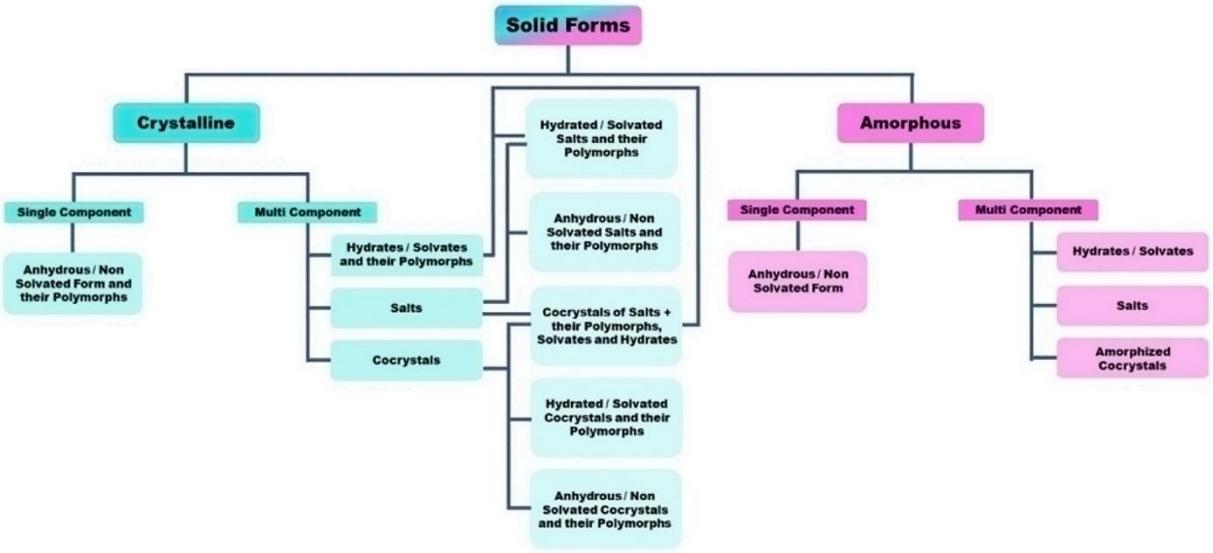

Figure 1. Different solid forms (adapted with permission from [2]. Copyright 2012 American Chemical Society.)

The vast majority of APIs demonstrating promising pharmacological properties in the early drug development stages are plagued by poor physico-chemical properties, such as poor stability, low aqueous solubility, low bioavailability, etc. These APIs consequently fail as novel chemical entities (NCE) for a number of clinical reasons. Additionally, due to their poor physico-chemical characteristics, the therapeutic potentials of these APIs could not be realized. Solid-state chemists respond to this situation by either screening an appropriate polymorphic form of the API or creating multi-component crystals such as its solvates, hydrates, and, more recently, co-crystals. While polymorph screening is a laborious and time-consuming operation, using solvates in the pharmaceutical industry is strongly discouraged since the organic solvent residue may harm human health. Hydrates also have several manufacturing and storage issues and are known to be less bioavailable compared to their anhydrous counterparts. The most popular method currently employed to alter the physico-chemical characteristics of an API is its salt formation. It is estimated that over half of the medications currently available in the market are in the salt form. However, a significant drawback of this strategy is that the API needs to have an appropriate (basic or acidic) ionizable site [3]. Co-crystallization presents a different strategy by which an API can potentially be co-crystallized, regardless of whether it contains basic, acidic, or ionizable groups. Another striking aspect of this strategy is the use of ‘co-formers’, which are basically FDA-approved, safe, food or pharmaceutical-grade additives with a variety of options to choose from [3]. The main advantage of synthesizing co-crystals is that along with the retention of the pharmacological properties, the physicochemical properties of the API can be improved by the incorporated co-former. The type of improvement is determined by the type of co-former selected.

The selection of a suitable co-former is the most important aspect of designing co-crystals, and it is usually done using either knowledge-based methods, computational approaches, or experimental methods. The most common knowledge-based methods utilized by researchers include hydrogen bonding propensity (HBP) evaluation [4], supramolecular synthon approach [5], molecular complementarity analysis using Cambridge structural database (CSD) [6], pKa rule [7], Hansen solubility parameter [8], etc. Computational approaches include *ab initio* molecular dynamic methods [9], machine learning models [10],

the use of artificial neural networks [11], lattice energy calculation [12] etc. In experimental methods, 'Hit and Trial' approach is employed with a variety of co-formers for the target API [13].

The experimental method of co-crystal screening is laborious, costly, and time-consuming. On the other hand, the prediction of co-crystal formation using a knowledge-based approach and computational methods is relatively fast and provides valuable information to guide the search for new co-crystal. However, these prediction methods have their own limitations and, when used solely, do not guarantee that co-crystals with predicted structures would form [14]. Moreover, the majority of these methods are based on complex methodologies, are not readily accessible, and demand high computational costs [15]. Thus, the interest in fast, greener, and reliable methods for screening new co-crystals has grown, and these methods can be performed with a small sample and commonly available methods. In this regard, well-established methods such as the identification of functioning supramolecular synthon [16, 17, 18], the 'pKa rule' [7,19], mechanochemical co-crystallization [20,21], solid-state analysis using differential scanning calorimetry (DSC) [22,23] and infrared spectroscopy (IR) [24] have shown to provide quick and effective evidence of co-crystal formation. A combination of these knowledge-based and experimental methods can be used to direct the search for novel co-crystals more reliably and efficiently.

After a successful co-former screening, the co-crystal is synthesized and primarily examined from a structural standpoint only. The studies on different thermodynamic aspects of co-crystals necessary for understanding their formation, stability, and dissolution are relatively scarce. Let us consider that n moles of co-former, A (host API) and m moles of co-former, B (guest molecule), combine to form co-crystal, C according to the reaction:

$$nA + mB \rightarrow A_nB_m = C \quad (1)$$

The fundamental property governing the thermodynamic stability of co-crystal at a specific temperature, T is Gibbs energy of co-crystal formation ($\Delta_f G_C$)

$$\Delta_f G_C = \Delta_f H_C - T\Delta_f S_C = G_C^S - G_A^S - G_B^S \quad (2)$$

where $\Delta_f H_C$ and $T\Delta_f S_C$ are the enthalpic and entropic contributions respectively.

A negative value of formation Gibbs energy ($\Delta_f G_C = -\text{ve}$) signifies that co-crystal, C is the stable phase with respect to a 1:1 mixture of its co-formers A and B at temperature T [25].

Many times, due to a lack of experimental techniques and computational cost, the calculation of $\Delta_f G_C$ is not realized. The majority of work on thermodynamic aspects of co-crystals involves a calculation of computationally inexpensive lattice energy and formation energy ($\Delta_f E_C = E_{latt}^C - (E_{latt}^A + E_{latt}^B)$). Under ambient conditions, the energy of formation is approximately equal to the enthalpy of formation ($\Delta_f E_C \approx \Delta_f H_C$). Correlating $\Delta_f E_C$ with co-crystal stability assumes that enthalpy is the major component of $\Delta_f G_C$ and the main driving force of co-crystallization. Nevertheless, entropically driven co-crystallization is also possible, as demonstrated by celecoxib-nicotinamide co-crystal [26]. Moreover, the literature claims that entropy determines the formation process of every third co-crystal [27]. Consequently, the study can provide a better understanding of the nature of co-crystallization, which includes information on all three formation thermodynamic functions [28]. In this regard, a predictive model developed by German L. Perlovich to estimate the formation thermodynamic characteristics of co-crystal can be useful [29-31]. A unique feature of this approach is that it requires the knowledge of the melting points of co-formers and co-crystal, which can be

quickly determined using routine DSC experiments whereas the necessary sublimation thermodynamic data of co-formers can be obtained by fitting vapor pressure data to the Clark-Glew equation [32].

In this work, a step-by-step approach towards co-crystal screening is elaborated using salicylic acid (SA) and benzamide (BZD) co-crystal systems. Salicylic acid [$C_7H_6O_3$; CAS Registry No. 69-72-7; Figure 2a] belongs to the class of drugs known as salicylates and is used to treat many skin disorders such as acne, dandruff, psoriasis, seborrheic dermatitis, corn, warts, etc. Benzamide [C_7H_7NO; CAS Registry No. 55-21-0; Figure 2b] and its derivatives also possess different kinds of pharmacological activities like antimicrobial, analgesic, anti-inflammatory, anticancer, cardiovascular, and other biological activities [33]. Two co-crystals of salicylic acid and benzamide (SA:BZD) involving stoichiometric diversity have been reported in the literature, i.e., SA:BZD (1:1) [34] and SA:BZD (1:2) [35]. In the second part of this work, the thermodynamic characteristics of SA:BZD (1:1) co-crystal is estimated by the approach proposed by Perlovich, which to the best of our knowledge, has not been previously attempted for this co-crystal.

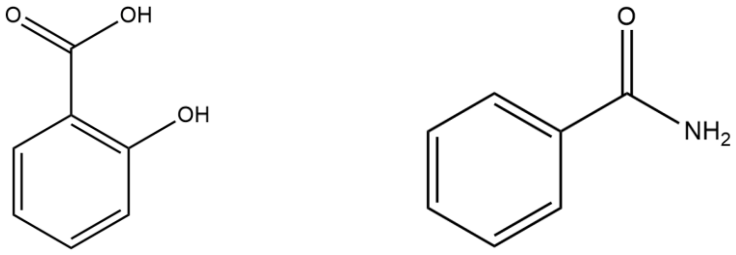

(a) **(b)**

Figure 2. (a) Molecular structure of SA ($C_7H_6O_3$); **(b)** molecular structure of BZD (C_7H_7NO).

For the estimation of the formation thermodynamic of co-crystals by Perlovich's approach, the knowledge of the melting points (T_{fus}) of co-crystals and their co-formers as well as sublimation thermodynamic functions of co-formers, is important. Melting point determination can be easily carried out by the routine DSC experiment. The thermodynamic functions of sublimation can be obtained by fitting the experimental vapor pressure (p) vs temperature (T) data to the Clarke-Glew equation of the type:

$$R\ln\left(\frac{p}{p^\circ}\right) = -\frac{\Delta^{g}_{cr}G^\circ_m(\theta)}{\theta} + \Delta^{g}_{cr}H^\circ_m(\theta)\left(\frac{1}{\theta}-\frac{1}{T}\right) + \Delta^{g}_{cr}C^\circ_{p,m}(\theta)\left[\left(\frac{\theta}{T}\right)-1+\ln\left(\frac{T}{\theta}\right)\right] \quad (3)$$

where p is the vapor pressure at the temperature T, P° is the selected reference pressure, R is the molar gas constant, $\Delta^{g}_{cr}G^\circ_m(\theta)$ and $\Delta^{g}_{cr}H^\circ_m(\theta)$ are the standard molar Gibbs energy and enthalpy of sublimation, respectively, at the selected reference temperature, θ and $\Delta^{g}_{cr}C^\circ_{p,m}(\theta)$ is the difference between the constant pressure standard molar heat capacity of gaseous phase and crystalline phase of the given compound at the reference temperature, θ. The advantage of Equation 3 is that the required sublimation thermodynamic functions can be directly obtained as fitting coefficients [36,37]. In this work the reference values are: $P^\circ = 10^5$ Pa, θ = 298.15 K, R = 8.31447 J·K^{-1}·mol^{-1}.

The relationship between vapor pressure (p) and temperature (T) is described by Antoine equation of the type:

$$\ln p = A - \frac{B}{C+T} \quad (4)$$

Where A, B, and C are Antoine coefficients. The vapor pressure in the given temperature range can be calculated if the Antoine coefficients are known.

The heat capacity adjustment $\Delta_{cr}^{g}C_{p,m}^{\circ}(\theta)$ is required in Equation 3 to adjust the sublimation thermodynamic function to 298.15 K. For this, the heat capacity of crystalline and gaseous phases of the compound is required, which is not readily available. The estimation of $\Delta_{cr}^{g}C_{p,m}^{\circ}(\theta)$ is thus performed by the empirical equation derived by Chickos *et al.* [38] of the type:

$$\Delta_{cr}^{g}C_{p,m}^{\circ}(\theta) = -\left[0.75 + 0.15\ C_{p,m}^{\circ}(\mathrm{Cr})\right] \mathrm{J \cdot K^{-1} \cdot mol^{-1}} \quad (5)$$

where $C_{p,m}^{\circ}(\mathrm{Cr})$ is the constant pressure heat capacity of the crystalline phase of the compound at 298.15 K.

For the purpose of subsequent calculations, the sublimation thermodynamic function ($\Delta_{cr}^{g}G_{m}^{\circ}(\theta)$ and $\Delta_{cr}^{g}H_{m}^{\circ}(\theta)$) obtained by Equation 3 at the specified reference values will be denoted as ΔG_{sub}^{298} and ΔH_{sub}^{298} respectively.

According to the literature, there is a linear relationship between ΔG_{sub}^{298} and T_{fus} for the structurally similar compounds as per the Tanimoto similarity coefficient. Regardless of the stoichiometry, the two-component co-crystal can be regarded as structurally equivalent to its individual co-formers. In other words, the experimental values of ΔG_{sub}^{298} vs T_{fus} for both co-formers and the co-crystal correspond to one and the same cluster. Thus, if the ΔG_{sub}^{298} and T_{fus} of both the co-formers are known, the coefficients of the linear regression, D and E can be obtained from the equation:

$$\Delta G_{sub}^{298} = D + E \cdot T_{fus} \quad (6)$$

The sublimation Gibbs energy of the co-crystal, $\Delta G_{sub}^{298}(CC)$ can be calculated using coefficients D and E, if the melting point of the co-crystal, $T_{fus}(\mathrm{CC})$ is known.

$$\Delta G_{sub}^{298}(CC) = D + E \cdot T_{fus}(\mathrm{CC}) \quad (7)$$

For the co-crystal of the type $(\mathrm{API})_n(\mathrm{CF})_m$, the sublimation Gibbs energy of the physical mixture $\Delta G_{sub}^{298}(\mathrm{PM})$ can be calculated from the equation:

$$\Delta G_{sub}^{298}(\mathrm{PM}) = X_1 \cdot \Delta G_{sub}^{298}(\mathrm{API}) + X_2 \cdot \Delta G_{sub}^{298}(\mathrm{CF}) \quad (8)$$

Here for the purpose of differentiating the co-formers, they are being denoted as API and CF. X_1 = n/(n+m), X_2 = m/(n+m), $\Delta G_{sub}^{298}(\mathrm{API})$ and $\Delta G_{sub}^{298}(\mathrm{CF})$ respectively are the sublimation Gibbs energies of API and co-former.

The formation Gibbs energy of co-crystal can now be calculated from the equation:

$$\Delta G_{f}^{298}(\mathrm{CC}) = \Delta G_{sub}^{298}(\mathrm{CC}) - \Delta G_{sub}^{298}(\mathrm{PM}) \quad (9)$$

The sublimation enthalpy of co-crystal can be calculated from the linear dependence between ΔG_{sub}^{298} and ΔH_{sub}^{298} (compensation effect).

$$\Delta G_{sub}^{298} = F + L \cdot \Delta H_{sub}^{298} \quad (10)$$

The sublimation enthalpy of the co-crystal, $\Delta H_{sub}^{298}(CC)$ can be calculated using coefficients F and L and $\Delta G_{sub}^{298}(CC)$, calculated previously.

$$\Delta H_{sub}^{298}(CC) = (\Delta G_{sub}^{298}(CC) - F)/L \quad (11)$$

The sublimation enthalpy of the physical mixture $\Delta H_{sub}^{298}(\mathrm{PM})$ is calculated as:

$$\Delta H_{sub}^{298}(\mathrm{PM}) = X_1 \cdot \Delta H_{sub}^{298}(\mathrm{API}) + X_2 \cdot \Delta H_{sub}^{298}(\mathrm{CF}) \quad (12)$$

Where $\Delta H_{sub}^{298}(\mathrm{API})$ and $\Delta H_{sub}^{298}(\mathrm{CF})$ are the sublimation enthalpies of API and co-former, respectively. The enthalpy of co-crystal formation can now be calculated from the equation:

$$\Delta H_{f}^{298}(\mathrm{CC}) = \Delta H_{sub}^{298}(\mathrm{CC}) - \Delta H_{sub}^{298}(\mathrm{PM}) \quad (13)$$

The entropy term is calculated as:

$$T\Delta S_{\mathrm{f}}^{298}(\mathrm{CC}) = \Delta H_{\mathrm{f}}^{298}(\mathrm{CC}) - \Delta G_{\mathrm{f}}^{298}(\mathrm{CC}) \quad (14)$$

2. Materials and Methods

2.1. Materials.

Salicylic acid (CDH, Purity – 99%, Mol. Wt. -138.12 g·mol^{-1}), Benzamide (Loba Chemie, Purity – 98%, Mol. Wt. – 121.14 g·mol^{-1}) and Ethanol (CSS Reagent, Purity – 99.9%) were used as received.

2.2. Methods.

2.2.1. Preparation of SA:BZD (1:1) physical mixture.

A 1:1 physical mixture of SA and BZD was prepared by carefully weighing equimolar amounts of both compounds, followed by gently mixing using mortar and pestle.

2.2.2. Preparation of SA:BZD co-crystals.

SA-BZD co-crystals were prepared by both liquid-assisted grinding (LAG) and solvent evaporation methods. In LAG, the calculated amount of SA and BZD were carefully weighed to achieve a 1:1 and 1:2 molar ratio. The compounds in the molar ratio were then manually ground using mortar and pestle with the addition of 500 µl of ethanol at regular intervals using a micropipette.

The synthesis of co-crystals using the solvent evaporation method was performed as given in the literature. The compounds were carefully weighed in the required molar ratio (1:1 and 1:2) and were then dissolved in ethanol with slight warming in order to achieve complete dissolution. The solutions were then filtered and allowed to evaporate slowly at room temperature. Crystals were formed over the course of 1 month.

2.3. Detection methods.

DSC analysis on salicylic acid, benzamide, physical mixture, and co-crystals was performed on Perkin Elmer DSC 6000. DSC was calibrated using certified zinc and indium reference materials. 2 to 6 mg of grounded samples were weighed and sealed in non-hermatic aluminum pans. Analysis was done at the heating rates of 1 and 5 K/min under dry nitrogen atmosphere with a flow rate 20 ml/s.

Infrared spectra of the co-former and synthesized co-crystals were directly collected on Perkin Elmer Spectrum Two™ spectrometer using Attenuated total reflection (ATR) without any further preparation. The spectrum was recorded in the range of 4000–500 cm^{-1}. The spectra obtained were interpreted for the presence of characteristic peaks.

Powder X-ray diffraction (XRPD) pattern of SA:BZD (1:1) co-crystal was collected on Bruker D8 Advance diffractometer (Cu Kα : λ = 1.54060 Å, 40 kV, 40 mA). The scanning was done at a 2θ range of 5 to 40 with a step size of 0.05°

2.4. Data analysis.

The fitting of the experimental vapor pressure (*p*) vs. temperature (*T*) data to the Clarke-Glew equation was performed on Origin by user defined non-linear curve fit. The calculation of formation thermodynamic functions for SA:BZD (1:1) co-crystal was performed on MS

Excel. The SA-BZD co-crystal structure visualizations were performed on Mercury software using a crystallographic information file (CIF) retrieved from CSD.

3. Results and Discussion

3.1. Co-crystal screening.

3.1.1. Identification of functioning supramolecular synthons.

In crystals, the structural units created by intermolecular interactions are known as supramolecular synthons. G.R. Desiraju, in 1995, defined the term supramolecular synthon as *"structural units within supermolecules which can be formed and/or assembled by known or conceivable synthetic operations involving intermolecular interactions"* [39]. M. Zaworotko expanded the idea of a supramolecular synthon into two different subcategories.

i. Supramolecular homosynthon: It results from the interaction between molecules with a similar self-complimentary functional group such as acid-acid dimer, amid-amide dimer, etc.
ii. Supramolecular heterosynthon: It results from the interaction between molecules with different but complimentary functional groups such as acid-amide, acid-pyridine, amide-pyridine, etc.

Suppose distinct and recognizable intermolecular interactions repeatedly arise for the given API and associated co-formers. In that case, they can be considered a functioning synthon and can provide a way to do co-crystal synthesis with a high level of reliability [16, 17, 18]. A CSD search reveals that the acid-amide is the most distinct and recognizable intermolecular interaction that frequently occurs for salicylic acid co-crystals (33% occurrence). Acid-amide interactions can occur in different ways, but the acid-amide heterodimer is the one that occurs in the majority of cases. Table 1 lists the co-crystals of salicylic acid and the applicable synthons. The acid-amide heterodimer synthon has been used extensively in crystal engineering due to the presence of strong and highly directional N-H•••••O=C and O-H•••••O=C hydrogen bonding interactions [40].

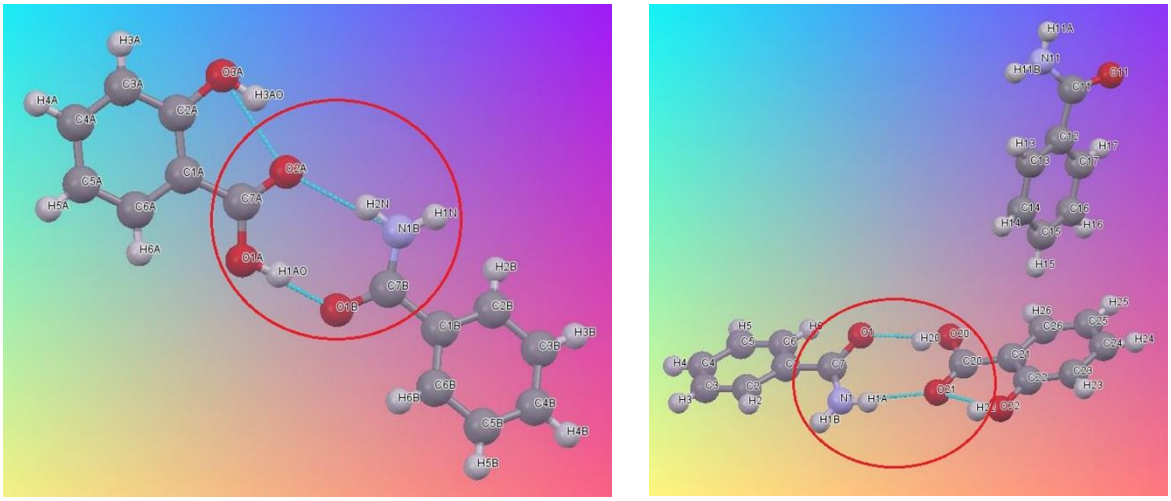

(a) **(b)**

Figure 3. Hydrogen-bonded acid-amide dimer in **(a)** SA-BZD (1:1) co-crystal; **(b)** SA-BZD (1:2) co-crystal.

In SA-BZD co-crystal, the primary structural unit is an acid-amide dimer established through hydrogen bonding (Figure 3). However, the occurrence of synthons cannot guarantee the formation of co-crystals. In the two independent studies conducted on acid-amide dimer

synthon, the influence of electron-donating and electron-withdrawing substituents on the acidic and basic characteristics of acid and amides, respectively, have been discussed [40,41]. Apart from the hydrogen-bonded dimer, the additional interactions within the crystal lattice can also favor co-crystal formation.

3.1.2. Selection of potential co-formers.

After identifying the prominent functioning synthons, the potential co-formers with complementary functional groups are searched. Benzamide as a co-former satisfies these criteria due to its capability to participate in prominent acid-amide interaction frequently observed for salicylic acid co-crystals. Secondly, the basic aim of co-crystallization of an API is to improve its physico-chemical properties. The solubility of salicylic acid is very low in water (2.2 g/l), which can affect its formulation and application. Benzamide, on the other hand, is fairly soluble in water (13 g/l). The solubilization of pharmaceutical co-crystal composed of poorly aqueous soluble API and water-soluble co-former involves three stages: (i) breaking of intermolecular bonds in co-crystal, (ii) breaking of intermolecular bonds in the solvent and (iii) formation of intermolecular bonds between co-crystal molecules and solvent molecules. It has been demonstrated that in the aqueous condition, the limiting step for the dissolution of poorly soluble API is solvation rather than it's breaking away from the co-crystal lattice. The co-former appears to reduce the solvation barrier of the poorly soluble API co-crystal to a level proportionate to the pure co-former. Hence, co-crystal solubility is related to co-former aqueous solubility [42]. Also, as previously discussed, benzamide and its derivatives have some antimicrobial activity that, when combined with salicylic acid, can be used to effectively manage skin-related disorders where monotherapy with salicylic acid or benzamide alone does not provide the desired result. SA-BZD co-crystal thus appears to offer an attractive proposition for combination therapy and to improve the solubility of poorly water-soluble salicylic acid.

3.1.3. Application of ΔpK_a rule for the identification of potential co-former:

The selected co-former will form salt or co-crystal with the given API, which is determined by the proton transfer. In the formation of salts, proton transfer is a distinct feature, whereas in the co-crystals, the proton is likely to be shared rather than transferred. It is generally accepted that an acid and a base will react to form salt if [ΔpK_a = pK_a (protonated base) − pK_a (acid)] > 3.75. This ΔpK_a rule is the result of years of experience gained in salt formulation within the pharmaceutical sector [7]. An extension to this rule for co-crystals containing acid-base pairs was proposed by Nangia *et al.* [43]. According to it, co-crystal formation will nearly always occur if the pK_a difference between the acidic and the basic components is less than 0.

$$[\Delta pK_a = pK_a(\text{protonated base}) - pK_a(\text{acid})] < 0 \quad (15)$$

ΔpK_a value greater than 3.75 ($\Delta pK_a > 3.75$) will result in salt; however, if the value lies between 0 and 3.75 ($0 < \Delta pK_a < 3.75$) the formation of salt or co-crystal cannot be accurately predicted. In this ΔpK_a region ($0 < \Delta pK_a < 3.75$), the position of the acid proton is significantly affected by the crystal structure of the complex, making it difficult to determine the proton position experimentally. Cruz-Cabeza derived a linear relationship between ΔpK_a and probability (P_{obs}) of co-crystal and salt formation in the ΔpK_a range $-1 < \Delta pK_a < 4$ [7]. The probability for acid and base to form co-crystal (AB) and salt (A-B+) can be estimated by the following equations:

$$P_{obs}(AB, \%) = -17 * \Delta pK_a + 72 \quad (16)$$

$$P_{obs}(A-B+,\%) = 17 * \Delta pK_a + 28 \quad (17)$$

Table 1. ΔpK_a Rule and Cruz-Cabeza model applied on representative salicylic acid co-crystal with applicable synthons.

Co-crystals of Salicylic acid	CSD Identifier	Synthon	ΔpK_a	P_{obs} (AB, %)	P_{obs} (A^-B^+, %)
Salicylic acid-Ethionamide	1958233	Acid-Pyridine	2.21	34.43	65.57
Salicylic acid-Theophylline	655945	Acid- Imidazole	-3.57		
Salicylic acid-Benzamide	756492	Acid-Amide	-3.99		
Salicylic acid-Isonicotinamide	1060737	Acid-Amide	0.66	60.78	39.22
Salicylic acid-Fluconazole	846646	Acid-Triazole	-0.49	80.33	19.67
Salicylic acid-Salicylamide	1545141	Acid-Amide	-3.76		
Salicylic acid-Temzolomide	881201	Acid-Amide	-6.39		
Salicylic acid-Antipyrine	1103434	Acid-Pyrazolone	-2.30		
Salicylic acid-Meloxicam	819113	Acid-Sulfathiazole	-2.32		
Salicylic acid-Lenvatinib	2008776	Acid-Pyridine	2.61	27.63	72.37
Salicylic acid-Caffeine	704929	Acid-Imidazole	-3.99		
Salicylic acid-Benznidazole	1563944	Acid-Imidazole	-2.59		
Salicylic acid-Isonicotinohydrazide	847204	Acid-Pyridine	0.56	62.48	37.52
Salicylic acid-Nicotinamide	767113	Acid-Amide	0.84	57.72	42.28
Salicylic acid-Tinidazole	1960462	Acid-Imidazole	0.49	63.67	36.33

pK_a : (Salicylic acid) = 2.79, (Ethionamide) = 5, (Theophylline) = -0.78, (Benzamide) = -1.2, (Isonicotinamide) = 3.45, (Flucanazole) = 2.3, (Salicylamide) = -0.97, (Temozolomide) = -3.6, (Antipyrine) = 0.49, (Meloxicam) = 0.47, (Lenvatinib) = 5.4, (Caffeine) = -1.2, (Benznidazole) = 0.2, (Isonicotinohydrazide) = 3.35 (Nicotinamide) = 3.63, (Tinidazole) = 3.28

pK_a values are derived from an aqueous environment, and using these values to make predictions for the potential proton transfer in solid-state can be impacted by the significant change in the solvation environment. Analysis of crystal structures from CSD has shown that when ΔpK_a is sufficiently negative (<−1) or sufficiently positive (> +4), the influence of the change in environment is unlikely to alter the prediction of salt/co-crystal formation using ΔpK_a rule. However, in the intermediate ΔpK_a range (-1 < ΔpK_a < 4), thermodynamic preferences for the proton transfer is strongly dependent on the solvation environment.

The values of ΔpK_a calculated from Equation 15 for different co-crystals of salicylic acid are compared in Table 1. In the majority of cases, it was found that the value of ΔpK_a was sufficiently negative (ΔpK_a < - 1), corresponding to the successful formation of co-crystals in these cases (53% occurrence), including SA-BZD co-crystal. In the intermediate ΔpK_a range (-1 < ΔpK_a < 4), the probability for the formation of co-crystal over salt, according to Equations 16 and 17 was higher for 5 out of 7 co-crystal systems (71% occurrence). Thus, overall, ΔpK_a rule was able to predict the formation of co-crystals of salicylic acid successfully.

3.1.4. Identification of co-crystal forming ability of API and co-former using Differential Scanning Calorimetry (DSC).

When heated, many organic binary mixtures form an eutectic melt. Eutectic melt, in turn, can produce co-crystals. Lu *et al.* hypothesized that when organic binary mixtures capable of forming eutectic are heated in DSC past the eutectic temperature, co-crystal formation can be easily facilitated [44]. In a typical DSC thermogram of eutectic forming a binary mixture, the appearance of an endothermic peak, followed by an exothermic peak corresponding to eutectic melting and crystallization of co-crystal from the melt, respectively, can be observed.

The appearance of an exothermic peak in the DSC profile is key evidence for the formation of co-crystal. An endothermic peak corresponding to the melting of co-crystal is also observed in DSC thermogram. Zhang *et al.*, based on their observations, proposed three models: Model A, which states that the appearance of three endotherms and two exotherms indicates co-crystal formation with stoichiometric diversity; Model B, which states that the appearance of two endotherms and one exotherm indicates co-crystal formation with a specific molar ratio; and Model C, which states that the appearance of one endotherm indicates no co-crystal formation. The use of slow heating rates is preferable to clearly differentiate the peaks associated with thermal events [45].

The DSC thermogram of SA:BZD (1:1) physical mixture (Figure 4a) is in accordance with Model A proposed by Zhang *et al.*, where three endotherms peaks (a, c, e) and two exothermic peaks (b, d) can be observed. The thermogram obtained using 5 K/min heating rate was not able to differentiate the first two endothermic peaks (Figure 4b). In Figure 4a, Peak (a) corresponds to the eutectic melt at $T_{m\text{-}E}$ = 378 K. Peak (a) is followed immediately by the crystallization of eutectic melt (peak (b)), which indicates the potential co-crystallization of a certain stoichiometry that subsequently melts (peak (c)) at T_f = 380 K. Peak (c) is followed by the crystallization of melt (peak (d)) that corresponds to the formation of co-crystals of different stoichiometry, subsequently melting (peak (e)) at T_f = 389 K. The observation of new endothermic and exothermic peaks and the disappearance of peaks due to the melting of co-formers (SA: T_f = 430 K ; BZD: T_f = 397 K) provides strong evidence for the formation of co-crystals from the physical mixture during heating [22]. Thus, DSC can be successfully applied to confirm co-crystal formation further. However, it should be noted that the interpretation of DSC results must be assisted by complementary techniques such as hot-stage microscopy (HSM) and XRPD. The composition of the eutectic melt can be determined by studying the variation in the enthalpies of fusion of eutectic melt as a function of the stoichiometry of the physical mixture (Tamman plot) [46].

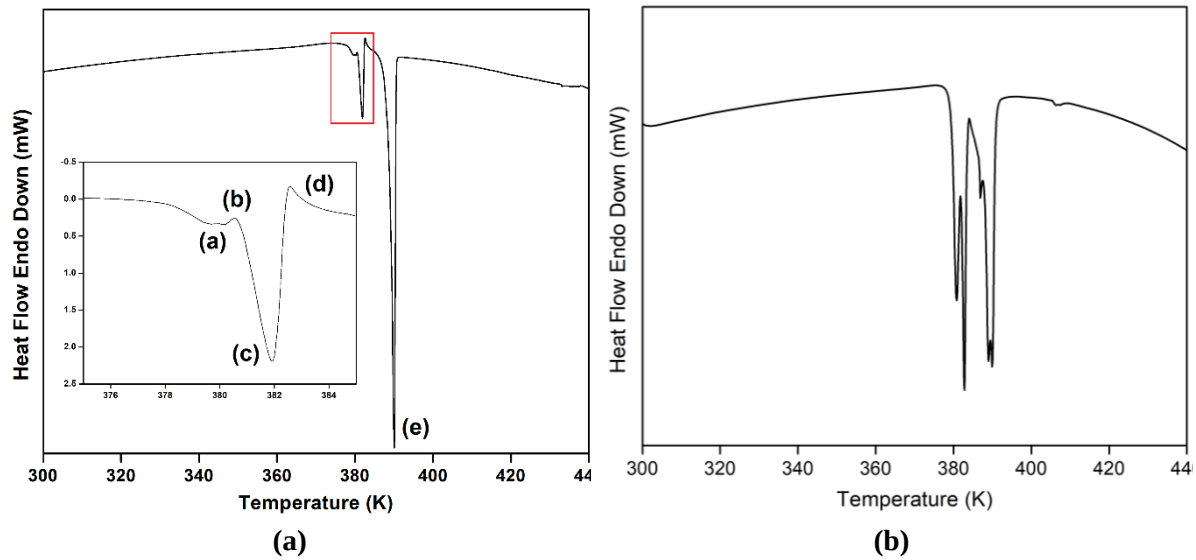

Figure 4. DSC thermogram of SA-BZD (1:1) physical mixture recorded at **(a)** 1 K/min heating rate showing three endotherms (peaks a, c and e) and two exotherms (peaks b and d); **(b)** 5 K/min heating rate.

3.1.5. Mechanochemical synthesis of co-crystal and its identification using Infrared Spectroscopy.

Mechanochemistry was recognized by IUPAC as one of the 10 inventions in chemistry that have the potential to change the world. It was given the moniker "chemical 2.0" as a good example of a green chemistry technique [14]. Mechanochemistry can also be utilized as an effective method for co-crystal preparation [21]. The simplest example of mechanochemical co-crystal formation is neat grinding, where two or more components are ground together. However, there are several examples where neat grinding results in incomplete reactions and non-accessible co-crystals. Liquid-assisted grinding (LAG) is an alternative to neat grinding, where mechanochemical productivity has been shown to increase significantly by adding a small amount of solvent. This approach has been helpful and convenient for obtaining co-crystals quickly compared to the solvent evaporation method.

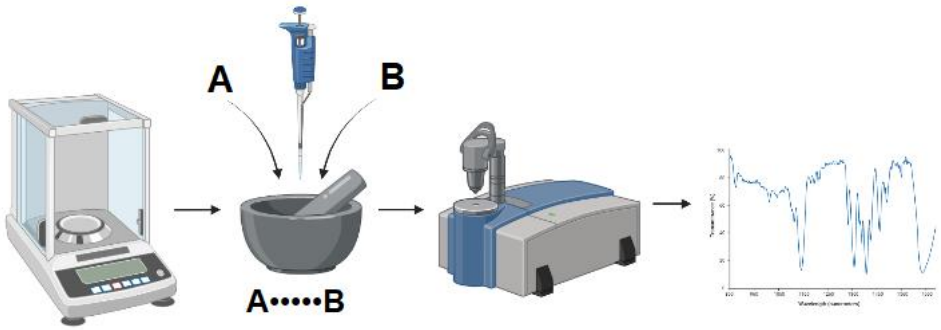

Figure 5. Illustration of mechanochemical synthesis of co-crystal and its identification using infrared spectroscopy.

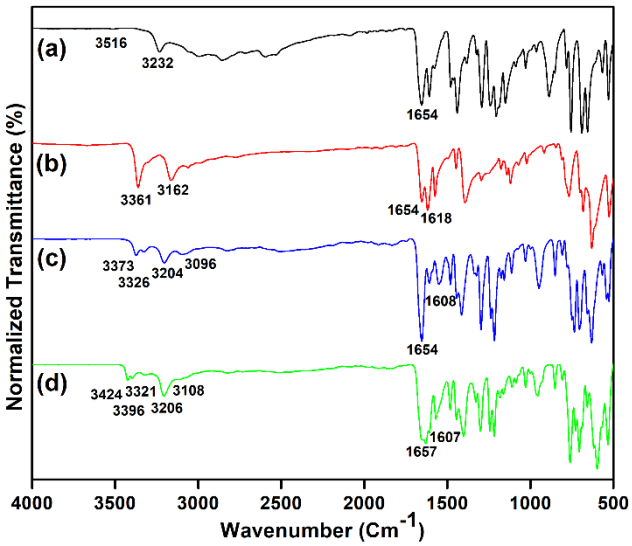

Figure 6. FTIR spectra of SA-BZD co-crystal system: **(a)** SA; **(b)** BZD; **(c)** SA-BZD (1:1); **(d)** SA-BZD (1:2).

The possible co-crystallization can then be confirmed by IR spectroscopy by comparing the IR spectra of pure co-formers with that of potential co-crystal samples formed by new hydrogen bonding between the two co-formers. The most noticeable are the peaks associated with the vibration of hydrogen bond donor and acceptor groups located in the functional group region of IR spectra. If there is a shift of these peaks relative to those of pure co-formers, it can be attributed to the hydrogen bond formation in the new co-crystal [47]. The vibration of hydrogen bond (DonorH•••••Acceptor) can also be found in IR spectrum. However, as these bonds are weak, their absorption peaks are typically located in the complicated fingerprint

region, where, due to the nature of the compounds studied, the assignment becomes very difficult [48].

SA:BZD (1:1) and SA:BZD (1:2) co-crystals prepared by manual liquid-assisted grinding were analyzed by IR spectroscopy, as illustrated in Figure 5. The IR spectra of pure co-formers and co-crystals in the region 4000 to 500 cm^{-1} are represented in Figure 6. It was found that the characteristic IR peaks of the co-crystals ($\nu_{OH}, \nu_{NH_2}, \nu_{C=O}, \delta_{NH_2}$) exhibited a shift to lower wavenumber compared to the pure co-formers (Table 2). This suggests that Acid-amide hydrogen bonding interactions in co-crystals are more stable and strong than acid-acid and amide-amide hydrogen bonding interactions in salicylic acid and benzamide.

Table 2. FTIR major band assignment of SA-BZD co-crystal system.

Sample	ν_{OH}	ν_{NH_2}	$\nu_{C=O}$	δ_{NH_2}
SA	3516 3232	–	1654	–
BZD	–	3361 3162	1654	1618
SA-BZD (1:1)	3373 3204	3204 3096	1654	1608
SA-BZD (1:2)	3424, 3396 3206	3206 3108	1657	1607

3.2. Synthesis of co-crystals using the solvent evaporation method.

SA-BZD (1:1) and SA:BZD (1:2) co-crystals were also synthesized using the solvent evaporation method. The obtained co-crystals were characterized by IR spectroscopy and DSC. The co-crystals obtained using the solvent evaporation method and liquid-assisted grinding were found to have identical IR spectra (Figures 7a and 7b). The melting points obtained for both the co-crystals using DSC were also identical to the endothermic events observed during the heating physical mixture (Figure 7c), thus providing conclusive evidence for the formation of stoichiometrically diverse SA-BZD co-crystals.

The thermodynamics of co-crystal formation was studied on SA-BZD (1:1) co-crystal. The experimental powder diffraction data collected on the co-crystal prepared by the solvent evaporation method was identical to the simulated diffraction pattern obtained from CIF (Figure 7d), confirming the phase purity.

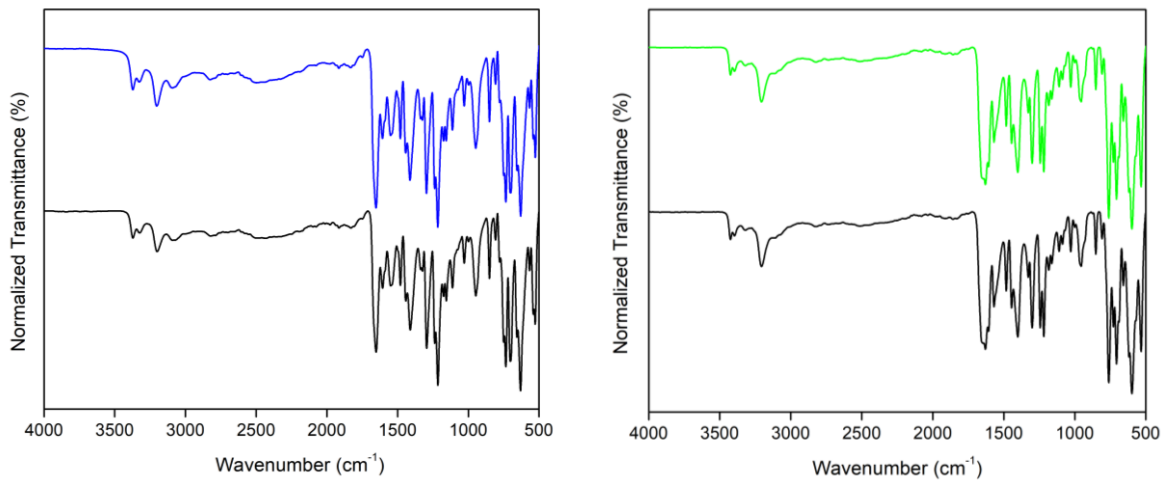

(a) **(b)**

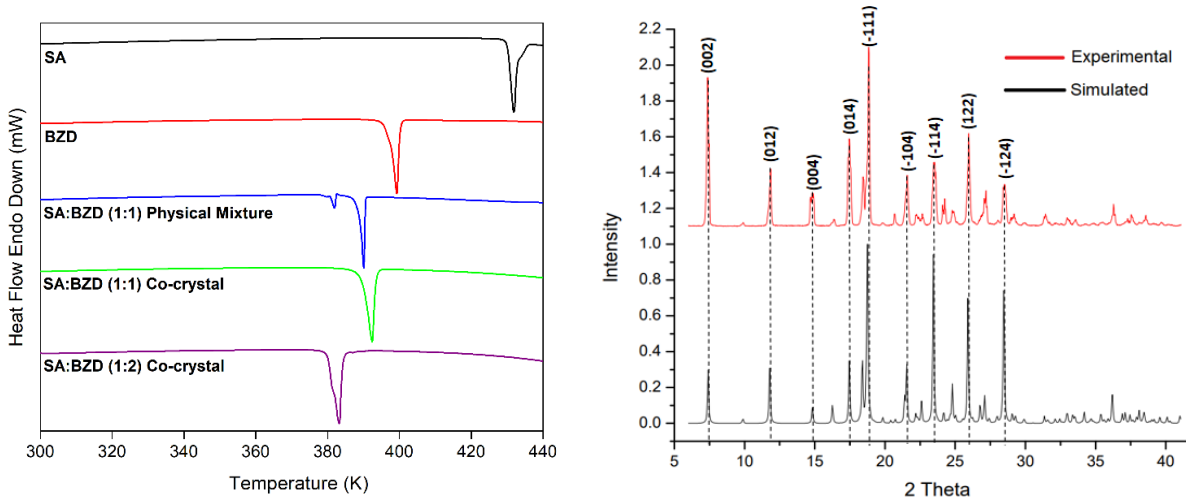

(c) **(d)**

Figure 7. FTIR spectra of SA-BZD co-crystal prepared by Liquid assisted grinding (colored) and solvent evaporation (black) for **(a)** SA-BZD (1:1); **(b)** SA-BZD (1:2); **(c)** DSC thermogram of co-formers and SA-BZD co-crystals; **(d)** comparison of experimental powder diffraction pattern with the simulated pattern for SA:BZD (1:1) co-crystal.

3.3. Formation thermodynamics of SA:BZD (1:1) co-crystal.

The formation of the thermodynamic functions of SA:BZD (1:1) co-crystal was estimated using the approach put forward by Perlovich. The necessary equations required for this estimation have been discussed in the theory section. The Antoine coefficients and the sublimation thermodynamic functions obtained as coefficients of Clarke-Glew fit (Figure 8) are given in Table 3.

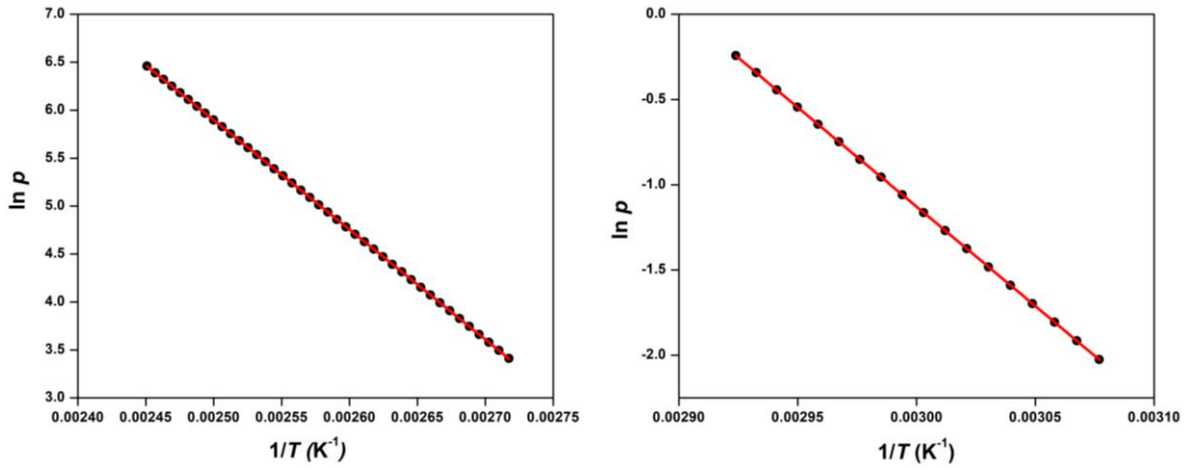

(a) **(b)**

Figure 8. Calculated ln *p* vs 1/T data using Antoine equation (●) and the fitted Clark-Glew equation (−) for **(a)** Salicylic acid (*T* = 368 – 408 K); **(b)** Benzamide (*T* = 325 – 342 K).

Table 3. Derived values and sublimation thermodynamics functions of salicylic acid (SA) and benzamide (BZD).

Co-former	Antoine Coefficients # (Eq. 4)			Chickos *et.al* (Eq. 5)	Clarke-Glew Fit (Eq. 3) *		
	A	B	C	$\Delta_{cr}^{g}C_{p,m}^{\circ}(\theta)$ **J·K⁻¹·mol⁻¹**	$\Delta_{cr}^{g}G_{m}^{\circ}(\theta)$ **kJ·mol⁻¹**	$\Delta_{cr}^{g}H_{m}^{\circ}(\theta)$ **kJ·mol⁻¹**	R^2
SA	34.50	11440.85	0	-24.89	38.414±0.005	97.347±0.021	0.9999
BZD	33.84	11657.75	0	-23.82	41.614±0.001	97.767±0.014	0.9999

The Antoine coefficient obtained from reference 49 for log base 10 formula was converted for natural log formula using the Environmental Model free tool ; * θ = 298.15 K, $p^{\circ} = 10^5$ Pa and R = 8.31447 J·K⁻¹·mol⁻¹

The melting points of co-former and co-crystal, the fitting coefficients, and the sublimation thermodynamic functions of SA-BZD (1:1) co-crystals and physical mixture are listed in Table 4.

Table 4. Melting points, coefficients of linear regression and sublimation thermodynamics of 1:1 co-crystal and physical mixture of salicylic acid (SA) and benzamide (BZD).

Co-former	T_{fus} / K *	Coefficients of Eq. 6 & 7		Coefficients of Eq. 10 & 11	
		D	E	F	L
SA	430.07	80.334	-0.0975	92.3	0.1314
BZD	397.24				
SA:BZD (1:1) Co-crystal	389.73	ΔG_{sub}^{298}(CC) (Eq. 7) kJ·mol^{-1}		ΔH_{sub}^{298}(CC) (Eq. 11) kJ·mol^{-1}	
		42.336		97.863	
SA:BZD (1:1) Physical Mixture		ΔG_{sub}^{298}(PM) (Eq. 8) kJ·mol^{-1}		ΔH_{sub}^{298}(PM) (Eq. 12) kJ·mol^{-1}	
		40.014		97.556	

*onset temperature of the melting peak obtained from DSC

The estimated formation thermodynamic functions for the SA-BZD (1:1) co-crystal are given in Table 5.

Table 5. Formation thermodynamic function of SA:BZD (1:1) co-crystal.

	ΔG_f^{298}(CC) (Eq. 9) kJ·mol^{-1}	ΔH_f^{298}(CC) (Eq. 13) kJ·mol^{-1}	$T\Delta S_f^{298}$(CC) (Eq. 14) kJ·mol^{-1}
SA:BZD (1:1) Co-crystal	2.322	0.306	-2.016

The estimated value of ΔG_f^{298}(CC) lies within the threshold value of 5 kJ·mol^{-1} (ΔG_f^{298}(CC) < 5 kJ·mol^{-1}) and meets the criteria of thermodynamically stable co-crystal. This reservation takes into account the different polymorphic modification available for the co-former (Benzamide has 4 polymorphs [50]) and the inherent problem in the selection of the right polymorphs for the calculation for which the sublimation data might not be available. The ΔH_f^{298}(CC) the term was positive and small compared to the $T\Delta S_f^{298}$(CC) term. The estimated formation thermodynamic functions follow the trend $\Delta H_f^{298} > 0, T\Delta S_f^{298} < 0, \left|T\Delta S_f^{298}\right| > \left|\Delta H_f^{298}\right|$ which accounts for entropy driven process [21]. A similar observation was made in a study by Seaton *et al.* where the calculated formation energy and the experimentally obtained enthalpy of formation of SA:BZD (1:1) co-crystal was found to be positive, indicating that the co-crystal is unfavoured compared to its co-formers. This was against the observation that both the co-formers in the co-crystal experience strong intermolecular interactions. Generally, the enthalpy term is expected to be negative for strong bonding interactions, favoring the co-crystal formation. The co-crystal's melting point is also lower than that of its co-formers (Table 4), which corresponds to a low enthalpy of formation. Thus, it was concluded that the crystal was entropically stabilized [33]. The predictive model developed by Perlovich was, therefore, able to correctly predict (at least qualitatively) the driving force for the SA:BZD (1:1) co-crystal formation.

4. Conclusions

In this work, a step-by-step methodology for co-crystal screening is elaborated on using SA-BZD co-crystal as a model system. The study illustrates the use of the Cambridge Structure

Database (CSD), the pKa rule, and commonly available analytical techniques such as DSC and IR to predict the formation of co-crystals successfully. The co-crystals were synthesized using the method reported in the literature. The melting points determined using DSC and the sublimation thermodynamic functions calculated using Clarke-Glew fit were used to estimate the formation thermodynamic functions of the SA:BZD (1:1) co-crystal. In line with the previous observation on this co-crystal system, the estimated thermodynamic function qualitatively affirms the co-crystal formation to be entropically driven. Also, as discussed in the introduction section, this work supports the notion that all three formation thermodynamic functions should be considered to better understand the nature of co-crystallization. Therefore, continuous research on prediction methods that can accurately predict co-crystallization from both structural and thermodynamic viewpoints is essential.

Funding

This research received no external funding.

Acknowledgments

Presented in 4th International Conference on "Recent Advances in Fundamental and Applied Sciences" (RAFAS-2023)" during March 24-25, 2023, Organized by the School of Chemical Engineering and Physical Sciences, Lovely Professional University, Punjab, India.
The services extended by the Central Instrumentation Facility (CIF), Lovely Professional University in the IR, XRPD, and DSC analysis are duly acknowledged.

Conflicts of Interest

The authors declare no conflict of interest.

References

1. Guan, D.; Xuan, B.; Wang, C.; Long, R.; Jiang, Y.; Mao, L.; Kang, J.; Wang, Z.; Chow, S.F.; Zhou, Q. Improving the Physicochemical and Biopharmaceutical Properties of Active Pharmaceutical Ingredients Derived from Traditional Chinese Medicine through Co-crystal Engineering. *Pharmaceutics* **2021**, *13*, 2160, https://doi.org/10.3390/pharmaceutics13122160.
2. Aitipamula, S.; Banerjee, R.; Bansal, A.K.; Biradha, K.; Cheney, M.L.; Choudhury, A.R.; ... Zaworotko, M.J. Polymorphs, salts, and co-crystals: what's in a name?. Cryst. Growth Des. **2012**, 12(5), 2147-2152, https://doi.org/10.1021/cg3002948
3. Schultheiss, N.; Newman, A. Pharmaceutical Co-crystals and Their Physicochemical Properties. *Cryst. Growth Des.* **2009**, *9*, 2950-2967, https://doi.org/10.1021/cg900129f.
4. Sarkar, N.; Sinha, A.S.; Aakeröy, C.B. Systematic investigation of hydrogen-bond propensities for informing co-crystal design and assembly. *CrystEngComm* **2019**, *21*, 6048-6055, https://doi.org/10.1039/C9CE01196J.
5. Sarma, J.A.R.P.; Desiraju, G.R. The Supramolecular Synthon Approach to Crystal Structure Prediction. *Cryst. Growth Des.* **2002**, *2*, 93-100, https://doi.org/10.1021/cg015576u.
6. Fábián, L. Cambridge Structural Database Analysis of Molecular Complementarity in Co-crystals. *Cryst. Growth Des.* **2009**, *9*, 1436-1443, https://doi.org/10.1021/cg800861m.
7. Cruz-Cabeza, A.J. Acid–base crystalline complexes and the pK_a rule. *CrystEngComm* **2012**, *14*, 6362-6365, https://doi.org/10.1039/C2CE26055G.
8. Mohammad, M.A.; Alhalaweh, A.; Velaga, S.P. Hansen solubility parameter as a tool to predict co-crystal formation. *Int. J. Pharm.* **2011**, *407*, 63-71, https://doi.org/10.1016/j.ijpharm.2011.01.030.
9. Barua, H.; Gunnam, A.; Yadav, B.; Nangia, A.; Shastri, N.R. An *ab initio* molecular dynamics method for co-crystal prediction: validation of the approach. *CrystEngComm* **2019**, *21*, 7233-7248, https://doi.org/10.1039/C9CE01436E.

10. Mswahili, M.E.; Lee, M.-J.; Martin, G.L.; Kim, J.; Kim, P.; Choi, G.J.; Jeong, Y.-S. Co-crystal Prediction Using Machine Learning Models and Descriptors. *Appl. Sci.* **2021**, *11*, 1323, https://doi.org/10.3390/app11031323.
11. Devogelaer, J.-J.; Meekes, H.; Tinnemans, P.; Vlieg, E.; de Gelder, R. Co-crystal Prediction by Artificial Neural Networks. *Angew. Chem. Int. Ed.* **2020**, *59*, 21711-21718, https://doi.org/10.1002/anie.202009467.
12. Kuleshova, L.N.; Hofmann, D.W.M.; Boese, R. Lattice energy calculation–A quick tool for screening of co-crystals and estimation of relative solubility. Case of flavonoids. *Chem. Phys. Lett.* **2013**, *564*, 26-32, https://doi.org/10.1016/j.cplett.2013.02.008.
13. Guo, M.; Sun, X.; Chen, J.; Cai, T. Pharmaceutical co-crystals: A review of preparations, physicochemical properties and applications. *Acta Pharm. Sin. B.* **2021**, *11*, 2537-2564, https://doi.org/10.1016/j.apsb.2021.03.030.
14. Guidetti, M.; Hilfiker, R.; Kuentz, M.; Bauer-Brandl, A.; Blatter, F. Exploring the Co-crystal Landscape of Posaconazole by Combining High-Throughput Screening Experimentation with Computational Chemistry. *Cryst. Growth Des.* **2022**, *23*, 842-852, https://doi.org/10.1021/acs.cgd.2c01072.
15. Dittrich, B.; Connor, L.E.; Werthmueller, D.; Sykes, N.; Udvarhelyi, A. Energy partitioning of pharmaceutical co-crystal structures. *CrystEngComm* **2023**, *25*, 1101-1115, https://doi.org/10.1039/D2CE00148A.
16. Aakeröy, C.B.; Sinha, A.S. Chapter 1: Co-crystals: Introduction and Scope. In Co-crystals: Preparation, Characterization and Applications; Aakeröy, C.B.; Sinha, A.S., Eds.; Royal Society of Chemistry, United Kingdom, **2018**, 1-32, https://doi.org/10.1039/9781788012874.
17. Cappuccino, C.; Cusack, D.; Flanagan, J.; Harrison, C.; Holohan, C.; Lestari, M.; Walsh, G.; Lusi, M. How many co-crystals are we missing? Assessing two crystal engineering approaches to pharmaceutical co-crystal screening. *Cryst. Growth Des.* **2022**, 22(2), 1390-1397, https://doi.org/10.1021/acs.cgd.2c00044.
18. Tupe, S.A.; Khandagale, S.P.; Jadhav, A.B. Pharmaceutical Co-crystals: An Emerging Approach to Modulate Physicochemical Properties of Active Pharmaceutical Ingredients. *J. Drug Deliv. Ther.* **2023**, *13*, 101-112, http://doi.org/10.22270/jddt.v13i4.6016.
19. Cruz-Cabeza, A.J.; Lusi, M.; Wheatcroft, H.P.; Bond, A.D. The role of solvation in proton transfer reactions: implications for predicting salt/co-crystal formation using the ΔpK_a rule. *Faraday Discuss.* **2022**, *235*, 446-466, https://doi.org/10.1039/D1FD00081K.
20. Ying, P.; Yu, J.; Su, W. Liquid-Assisted Grinding Mechanochemistry in the Synthesis of Pharmaceuticals. *Adv. Synth. Catal.* **2021**, *363*, 1246-1271, https://doi.org/10.1002/adsc.202001245.
21. Gröls, J.R.; Castro-Dominguez, B. Mechanochemical co-crystallization: Insights and predictions. *Comput. Chem. Eng.* **2021**, *153*, 107416, https://doi.org/10.1016/j.compchemeng.2021.107416.
22. Saganowska, P.; Wesolowski, M. DSC as a screening tool for rapid co-crystal detection in binary mixtures of benzodiazepines with co-formers. *J. Therm. Anal. Calorim.* **2018**, *133*, 785-795, https://doi.org/10.1007/s10973-017-6858-3.
23. Manin, A.N.; Voronin, A.P.; Drozd, K.V.; Manin, N.G.; Bauer-Brandl, A.; Perlovich, G.L. Co-crystal screening of hydroxybenzamides with benzoic acid derivatives: A comparative study of thermal and solution-based methods. *Eur. J. Pharm. Sci.* **2014**, *65*, 56-64, https://doi.org/10.1016/j.ejps.2014.09.003.
24. da Silva, C.C.; Guimarães, F.F.; Ribeiro, L.; Martins, F.T. Salt or cocrystal of salt? Probing the nature of multi-component crystal forms with infrared spectroscopy. *Spectrochim. Acta A Mol. Biomol. Spectrosc.* **2016**, *167*, 89-95, https://doi.org/10.1016/j.saa.2016.05.042.
25. Svärd, M.; Ahuja, D.; Rasmuson, Å.C. Calorimetric Determination of Co-crystal Thermodynamic Stability: Sulfamethazine–Salicylic Acid Case Study. *Cryst. Growth Des.* **2020**, *20*, 4243-4251, https://doi.org/10.1021/acs.cgd.9b01253.
26. Zhang, S.-W.; Brunskill, A.P.J.; Schwartz, E.; Sun, S. Celecoxib–Nicotinamide Co-crystal Revisited: Can Entropy Control Co-crystal Formation?. *Cryst. Growth Des.* **2017**, *17*, 2836-2843, https://doi.org/10.1021/acs.cgd.7b00308.
27. Perlovich, G.L. Two-component molecular crystals: relationship between the entropy term and the molecular volume of co-crystal formation. *CrystEngComm* **2018**, *20*, 3634-3637, https://doi.org/10.1039/C8CE00592C.
28. Surov, A.O.; Voronin, A.P.; Drozd, K.V.; Volkova, T.V.; Vasilev, N.; Batov, D.; Churakov, A.V.; Perlovich, G.L. Extending the Range of Nitrofurantoin Solid Forms: Effect of Molecular and Crystal Structure on Formation Thermodynamics and Physicochemical Properties. *Cryst. Growth Des.* **2022**, *22*, 2569-2586, https://doi.org/10.1021/acs.cgd.2c00044.

29. Perlovich, G.L. Two-component molecular crystals: relationship between the entropy term and the molecular volume of co-crystal formation. *CrystEngComm* **2018**, 20(26), 3634-3637, https://doi.org/10.1039/C5CE00992H.
30. Perlovich, G.L. Two-component molecular crystals: evaluation of the formation thermodynamics based on melting points and sublimation data. *CrystEngComm* **2017**, *19*, 2870-2883, https://doi.org/10.1039/C7CE00554G.
31. Manin, A.N.; Boycov, D.E.; Simonova, O.R.; Volkova, T.V.; Churakov, A.V.; Perlovich, G.L. Formation Thermodynamics of Carbamazepine with Benzamide, Para-Hydroxybenzamide and Isonicotinamide Co-crystals: Experimental and Theoretical Study. *Pharmaceutics* **2022**, *14*, 1881, https://doi.org/10.3390/pharmaceutics14091881.
32. Clarke, E.C.W.; Glew, D.N. Evaluation of thermodynamic functions from equilibrium constants. *Trans. Faraday Soc.* **1966**, *62*, 539-547, https://doi.org/10.1039/TF9666200539.
33. Tuğrak, M.; GÜl, H.İ.; Anil, B.; GÜlÇİn, İ. Synthesis and pharmacological effects of novel benzenesulfonamides carryingbenzamide moiety as carbonic anhydrase and acetylcholinesterase inhibitors. *Turk. J. Chem.* **2020**, *44*, 1601-1609, https://doi.org/10.3906/kim-2007-37.
34. Elbagerma, M.A.; Edwards, H.G.M.; Munshi, T.; Scowen, I.J. Identification of a new co-crystal of salicylic acid and benzamide of pharmaceutical relevance. *Anal. Bioanal. Chem.* **2010**, *397*, 137-146, https://doi.org/10.1007/s00216-009-3375-7.
35. Zhou, Z.; Chan, H.M.; Sung, H.H.-Y.; Tong, H.H.Y.; Zheng, Y. Identification of New Co-crystal Systems with Stoichiometric Diversity of Salicylic Acid Using Thermal Methods. *Pharm. Res.* **2016**, *33*, 1030-1039, https://doi.org/10.1007/s11095-015-1849-1.
36. Verevkin, S.P. Weaving a web of reliable thermochemistry around lignin building blocks: phenol, benzaldehyde, and anisole. *J. Therm. Anal. Calorim.* **2022**, *147*, 6073–6085, https://doi.org/10.1007/s10973-021-10924-x.
37. Mianowski, A.; Urbańczyk, W. Thermal dissociation in terms of the second law of chemical thermodynamics. *J. Therm. Anal. Calorim.* **2016**, *126*, 863-870, https://doi.org/10.1007/s10973-016-5569-5.
38. Chickos, J.S.; Hosseini, S.; Hesse, D.G.; Liebman, J.F. Heat capacity corrections to a standard state: a comparison of new and some literature methods for organic liquids and solids. *Struct. Chem.* **1993**, *4*, 271-278, https://doi.org/10.1007/BF00673701.
39. Desiraju, G.R. Supramolecular Synthons in Crystal Engineering—A New Organic Synthesis. *Angew. Chem. Int. Ed. Engl.* **1995**, *34*, 2311-2327, https://doi.org/10.1002/anie.199523111.
40. Saha, S.; Desiraju, G.R. Acid···Amide Supramolecular Synthon in Co-crystals: From Spectroscopic Detection to Property Engineering. *J. Am. Chem. Soc.* **2018**, *140*, 6361-6373, https://doi.org/10.1021/jacs.8b02435.
41. Seaton, C.C.; Parkin, A. Making Benzamide Co-crystals with Benzoic Acids: The Influence of Chemical Structure. *Cryst. Growth Des.* **2011**, *11*, 1502-1511, https://doi.org/10.1021/cg101403j.
42. Kuminek, G.; Cao, F.; da Rocha, A.B.d.O.; Cardoso, S.G.; Rodríguez-Hornedo, N. Co-crystals to facilitate delivery of poorly soluble compounds beyond-rule-of-5. *Adv. Drug Deliv. Rev.* **2016**, *101*, 143-166, https://doi.org/10.1016/j.addr.2016.04.022.
43. Bhogala, B.R.; Basavoju, S.; Nangia, A. Tape and layer structures in co-crystals of some di-and tricarboxylic acids with 4,4′-bipyridines and isonicotinamide. From binary to ternary co-crystals. *CrystEngComm* **2005**, *7*, 551-562, https://doi.org/10.1039/B509162D.
44. Lu, E.; Rodríguez-Hornedo, N.; Suryanarayanan, R. A rapid thermal method for co-crystal screening. *CrystEngComm* **2008**, *10*, 665-668, https://doi.org/10.1039/B801713C.
45. Zhou, Z.; Chan, H.M.; Sung, H.H.-Y.; Tong, H.H.Y.; Zheng, Y. Identification of New Co-crystal Systems with Stoichiometric Diversity of Salicylic Acid Using Thermal Methods. *Pharm. Res.* **2016**, *33*, 1030-1039, https://doi.org/10.1007/s11095-015-1849-1.
46. Vasilev, N.A.; Surov, A.O.; Voronin, A.P.; Drozd, K.V.; Perlovich, G.L. Novel co-crystals of itraconazole: Insights from phase diagrams, formation thermodynamics and solubility. *Int. J. Pharm.* **2021**, *599*, 120441, https://doi.org/10.1016/j.ijpharm.2021.120441.
47. González-González, J.S.; Jiménez-López, R.; Ortegón-Reyna, D.; Gonzalez-Carrillo, G.; Martínez-Martínez, F.J. Mechanochemical Synthesis of the Catechol-Theophylline Cocrystal: Spectroscopic Characterization and Molecular Structure. *Appl. Sci.* **2021**, *11*, 3810, https://doi.org/10.3390/app11093810.
48. Issa, N. Towards more Efficient Screening of Pharmaceutical Co-crystals, Ph.D. Thesis, Department of Chemistry, University College London, London, United Kingdom, **2011**.

49. Stephenson R.M.; Malanowski, S. Handbook of the Thermodynamics of Organic Compounds, Elsevier Science Publishing Co., New York; **1987**, 14-552, https://doi.org/10.1007/978-94-009-3173-2.
50. Fellah, N.; Shtukenberg, A.G.; Chan, E.J.; Vogt-Maranto, L.; Xu, W.; Li, C.; Tuckerman, M.E.; Kahr, B.; Ward, M.D. Disorderly Conduct of Benzamide IV: Crystallographic and Computational Analysis of High Entropy Polymorphs of Small Molecules. *Cryst. Growth Des.* **2020**, *20*, 2670-2682, https://doi.org/10.1021/acs.cgd.0c00096.